

Transformation of a tungsten wire to the plasma state by nanosecond electrical explosion in vacuum

G. S. Sarkisov

Ktech Corporation, Albuquerque, 10800 Gibson Blvd., New Mexico 87123, USA

S. E. Rosenthal and K. W. Struve

Sandia National Laboratories, Albuquerque, New Mexico 87110, USA

(Received 8 January 2008; published 14 May 2008; corrected 28 May 2008)

Experiment demonstrates the first direct transformation of a tungsten wire core to the plasma state by Joule heating during nanosecond electrical explosion in vacuum. Energy of ~ 130 eV/atom was deposited into the $12\ \mu\text{m}$ W wire coated by $2\ \mu\text{m}$ polyimide during the first ~ 10 ns. All the metal rapidly transformed to highly ionized plasma, while the surrounding polyimide coating remained primarily in a gaseous state. This coating totally suppressed corona formation. The expansion velocity of the wire was $\sim 12\text{--}18$ km/s, the average wire ionization at 50 ns reached $\sim 67\%$ with corresponding LTE temperature of ~ 1.2 eV. Explosion of bare W wire demonstrated earlier termination of the wire core heating due to shunting corona generation. Magnetohydrodynamic (MHD) simulation reproduces the main features of coated and uncoated W wire explosion.

DOI: [10.1103/PhysRevE.77.056406](https://doi.org/10.1103/PhysRevE.77.056406)

PACS number(s): 52.59.Qy, 52.65.Kj, 52.70.Ds, 52.70.Kz

I. INTRODUCTION

Modern exploding-wire research covers more than a half century. A comprehensive review of the earlier period in modern exploding-wire investigations was done in 1968 by Bennett [1] and by Lebedev and Savvatimskii [2] in 1984. Later, in 1990, Burtsev, Kalinin, and Luchinski published a book [3] that emphasized computer MHD modeling of exploding-wire phenomena. Electrical explosion of thin metal wire in vacuum can be described by a sequence of three processes [4]: (1) Current flows through the wire and Joule heats the metal; (2) Vapor ablated from the hot wire surface breaks down, producing a hot, fast expanding low-density corona; and (3) Joule heating of the wire core terminates due to radial switching of the current to the lower-resistance corona. The wire becomes a two-phase object: a cold core (~ 1 eV) containing almost all of the original mass and conducting negligible current, and a hot corona (~ 100 eV) with very small mass ($\sim 0.1\%$ of the original wire mass) and conducting most or all of the current. Further heating and ablating of the wire core occur only by heat transport and/or radiation from the hot surrounding plasma. Tungsten's high melting temperature and its strong electronic emitting property in conjunction with the presence of easily vaporized hydrocarbon impurities on the wire surface are responsible for earlier, premelt breakdown. This cold breakdown of tungsten wires was first pointed out as early as 1947 [5]. Exploding tungsten wires immersed in water or oil [2] avoids the earlier shunting breakdown and deposits more energy into the wire core. It was shown in Ref. [6] that fast explosion ($dI/dt \sim 150$ A/ns) in vacuum of tungsten wire with thin dielectric coating results in the total suppression of corona generation. Slower energy deposition ($dI/dt \sim 13$ A/ns) into coated W wire allows 2–3 times more energy deposition than into uncoated wire [7] but does not suppress corona generation (deposited energy 30%–40% of W atomization enthalpy, expansion velocity ~ 0.8 km/s, heating time ~ 70 ns).

This paper presents the first observation of the transformation of the entire tungsten wire with dielectric coating to the plasma state during corona-free electrical explosion in vacuum. Similar time-scale explosion of the corresponding bare wire results in corona generation with $\sim 1/3$ of the energy deposition.

II. EXPERIMENTAL SETUP

The experimental setup is based on a high-voltage trigger generator MAXWELL TG-70 (0.1 μF capacitor, charging voltage up to 70 kV, internal SF_6 gas switch). The trigger generator was connected to the coaxial target unit via 7 m of RG-218 cable. Current and voltage were measured with a 1.2-GHz-bandwidth coaxial shunt and a fast V dot. The coaxial vacuum target unit was described in [8]. The vacuum chamber was evacuated to 10^{-4} torr pressure to avoid breakdown. All wave forms were captured by a Tektronix TDS5104B 1-GHz four-channel digital oscilloscope. Figure 1 shows the optical-diagnostics setup. A short-pulse laser (EKSPLA-312, 100 mJ, 532 nm, 150 ps, 1 ns jitter) was used as the backlighting source for interferometry, shadowgraphy, and schlieren diagnostics. We employed a radial knife-edge schlieren scheme [9] that translates the regions with plasma refractivity ($\mu < 1$) and gas-type refractivity ($\mu > 1$) to separate areas of the schlieren image. A side-shearing air wedge interferometer [10] was used to obtain the interferogram and shadowgram on the same camera. To reduce optical aberration the angle plane of the glass wedge was placed orthogonal to the beam-splitting plane.

III. EXPERIMENTAL RESULTS

A. Explosion of coated tungsten wire

Figure 2 demonstrates the current, resistive voltage, and light emission wave forms for an exploding W wire with dielectric coating (shot 0222-02, 0.56 cm length, $12\ \mu\text{m}$ core diameter with $2\ \mu\text{m}$ polyimide coating). The voltage

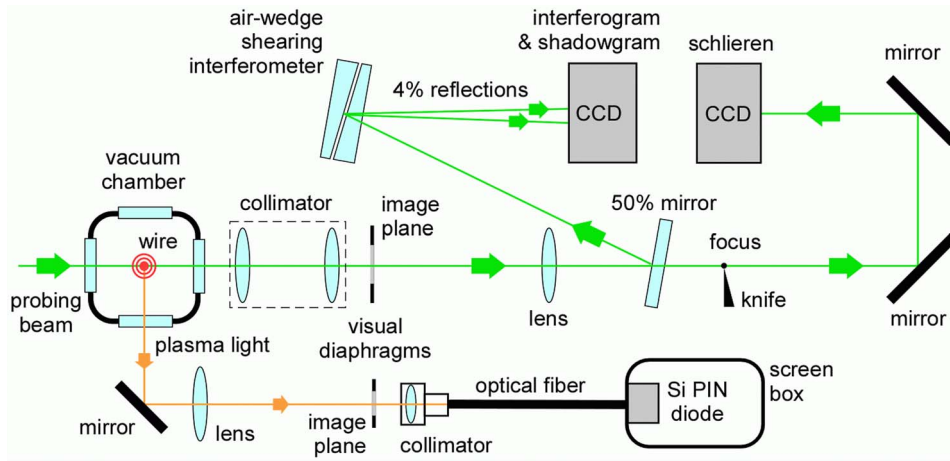


FIG. 1. (Color online) Optical setup.

took only ~ 3 ns of fast rise ($dV/dt \sim 50$ kV/cm ns) to reach its maximum value of ~ 150 kV/cm. The average rate of current rise was ~ 1 kA/ns. The maximum electrical power reached ~ 160 MW. The light wave form does not exhibit the narrow emission peak that accompanies breakdown [8]. The MHD-simulated voltage matches the rise of the experimental voltage, giving $\sim 13\%$ larger amplitude. Half-width and half-maximum of the MHD voltage is ~ 5 ns. The simulation produces an exponential tail, while the experimental voltage drops faster with an oscillatory component; but, generally, the fit is reasonable. According to the MHD simulation, specific energy ~ 130 eV/atom (68 kJ/g, 0.84 J) was deposited into the wire core. This is about 15 times the atomization enthalpy of W (~ 8.6 eV/atom) or the specific energy of TNT (4.2 kJ/g). In some experiments we have observed a strong short-time overvoltage accompanied by abnormally strong electromagnetic pulse. The reason for this overvoltage was inappropriate insulation of the power cable with the vacuum coaxial target unit. Oiling of the cable contact totally eliminated this overvoltage effect. Probably this cable-related breakdown can explain the strong overvoltage reported in Ref. [6].

Interferogram (a), shadowgram (b), and schlieren (c) images are presented in Fig. 3 for an exploding W wire with polyimide coating at a probing time of 50 ns after current rise (shot 0222-02). The images indicate a wire that expands in the form of a cylinder with sharp edges. This cylindrical structure is evidence of an axially uniform deposition of energy to the wire. Compression of the interference lines from the left side of the wire axis and expansion from the right side corresponds to the plasma type of refractivity ($\mu < 1$). The schlieren image shows a bright and wide axial stripe from the left side of the wire axis (plasma type of W refractivity), a narrow axial line from the right side of the wire axis (gas type of polyimide refractivity), and short axial right-sided stripes at the cathode and anode (gas type of W refractivity). The location with the notation “ZERO refraction” shows the region where the gas refractivity ($\mu > 1$) was compensated by the plasma’s refractivity ($\mu < 1$). In this region the electromagnetic wave propagates without refraction. The wire core size in the shadowgram at the moment of probing yields an estimated expansion velocity of ~ 12 km/s. This velocity is ~ 2.3 times larger than the speed of sound in solid tungsten ($V_{\text{sound}} \sim 5.2$ km/s).

Figure 4 shows the reconstruction of the interference phase shift along the radial line A-A in Fig. 3(a). The central part of the exploded wire (~ 1 mm diameter) exhibits a large negative phase shift $\delta_{\text{max}} \sim -1.1 \pm 0.1$ lines (plasma-type refractivity), while the periphery produces a small positive phase shift with maximum value $\sim 0.25 \pm 0.1$ lines (gas-type refractivity). Maximum expansion velocity of the phase disturbance is ~ 18 km/s. Calculating the phase shift radial profile from the MHD-simulation density and ionization profiles also shows plasma-type refractivity inside and gas type outside the metal core.

B. Explosion of uncoated tungsten wire

Current, resistive voltage, and light emission wave forms for the exploding bare W wire (shot 0125-07, 0.53 cm length, $12 \mu\text{m}$ diameter) are presented in Fig. 5. Similar to the exploding coated wire of Sec. III A, the average rate of current rise was ~ 1 kA/ns. The voltage reached its maximum value of ~ 175 kV/cm in ~ 5 ns. The maximum electrical power reached ~ 155 MW. The light wave form exhibited the nar-

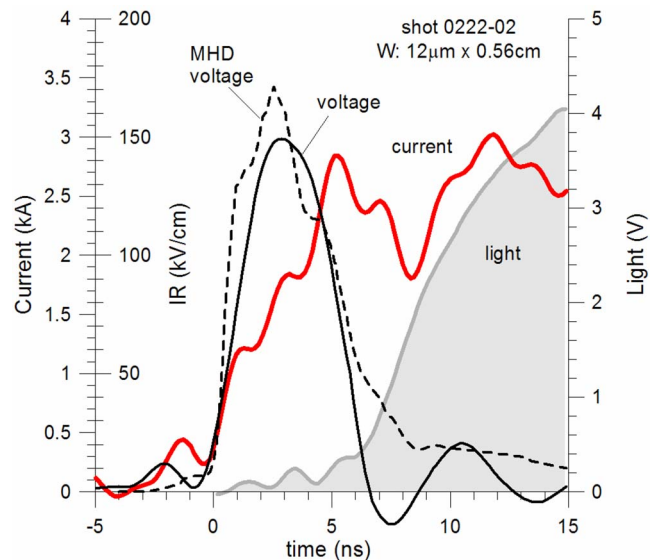


FIG. 2. (Color online) Current, voltage, and light emission wave forms for exploding $12 \mu\text{m}$ W wire with $2 \mu\text{m}$ polyimide coating.

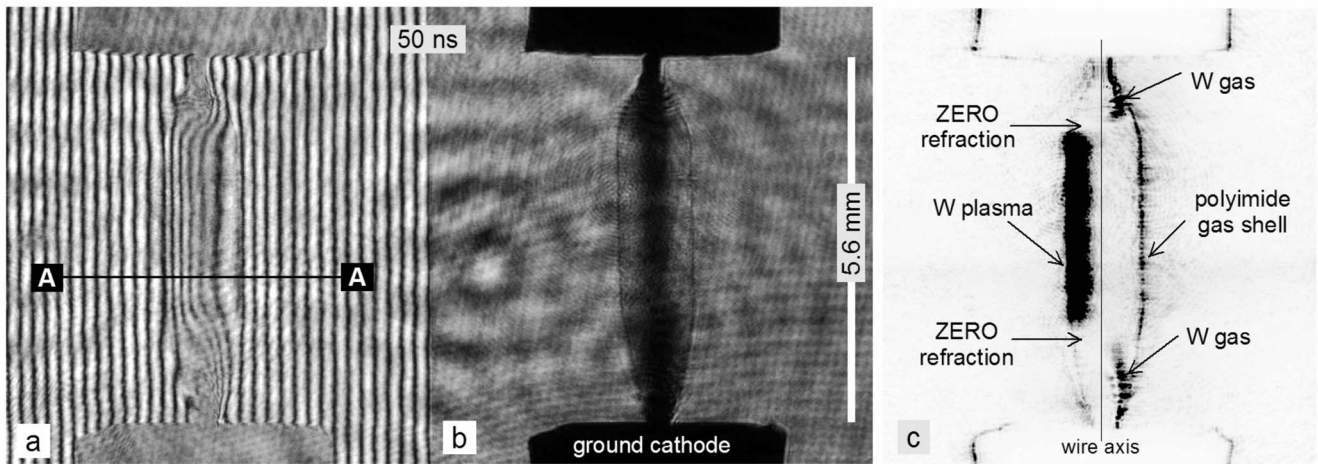


FIG. 3. Interferogram, shadowgram, and schlieren images of exploding 12 μm W wire with 2 μm polyimide coating.

row 3–4 ns duration emission peak that accompanies breakdown [8]. The MHD-simulated voltage matches the rise of the experimental voltage, giving $\sim 5\%$ larger amplitude. The simulation voltage demonstrates reasonable fit to the experimental one, but narrower with ~ 1.5 ns FWHM. According to MHD simulation, specific energy of ~ 26 eV/atom (14 kJ/g, 0.17 J) was deposited into the wire core (electrical power integration was stopped when the resistance dropped to half of its maximum value, as described in Ref. [4]). This is almost three times the atomization enthalpy of W and the specific energy of TNT. We need to point out that the 1 GHz Tektronix is not fast enough to resolve a 1.5 ns voltage spike (the dV/dt signal is at least twice as fast as V). Hence, our voltage measurement is unable to correctly capture a voltage like that generated by the MHD simulation.

Figure 6 shows the interferogram (a), shadowgram (b), and schlieren (c) images for an exploding bare W wire (shot

0125-07) at a probing time of 170 ns after the current rise. The images indicate a conical expansion of the wire core directed to the high-voltage anode. This conical structure is evidence of axially increasing energy deposition toward the anode due to the polarity effect [11]. Compression of the interference lines from the right side of the wire axis and decompression from the left side corresponds to the gas type of refractivity ($\mu > 1$). The schlieren image 6(c) shows a bright and wide internal axial stripe from the right side of the wire axis which corresponds to gas type of refractivity for the wire core. The shadowgram 6(b) shows the signature of a shock wave structure at the cathode. The narrow bright stripe on the left side of the wire axis on schlieren image 6(c) indicates the plasma nature of this cathode phase disturbance. The wire core size at the moment of probing yields an estimated expansion velocity of 4–6 km/s. These detailed optical diagnostics clearly show that, in sharp contrast to the coated wire, the explosion of 12 μm bare W wire does not transform the metal core predominantly to the plasma state.

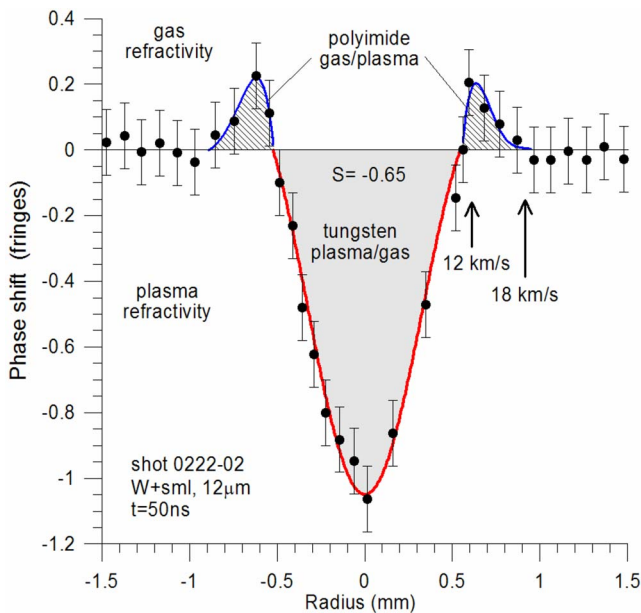


FIG. 4. (Color online) Interference phase shift in radial cross section A-A.

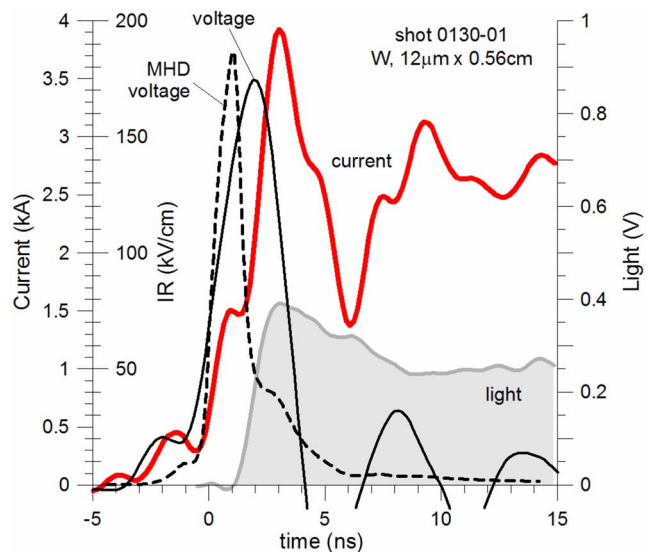


FIG. 5. (Color online) Current, voltage, and light emission wave forms for exploding 12 μm bare W wire.

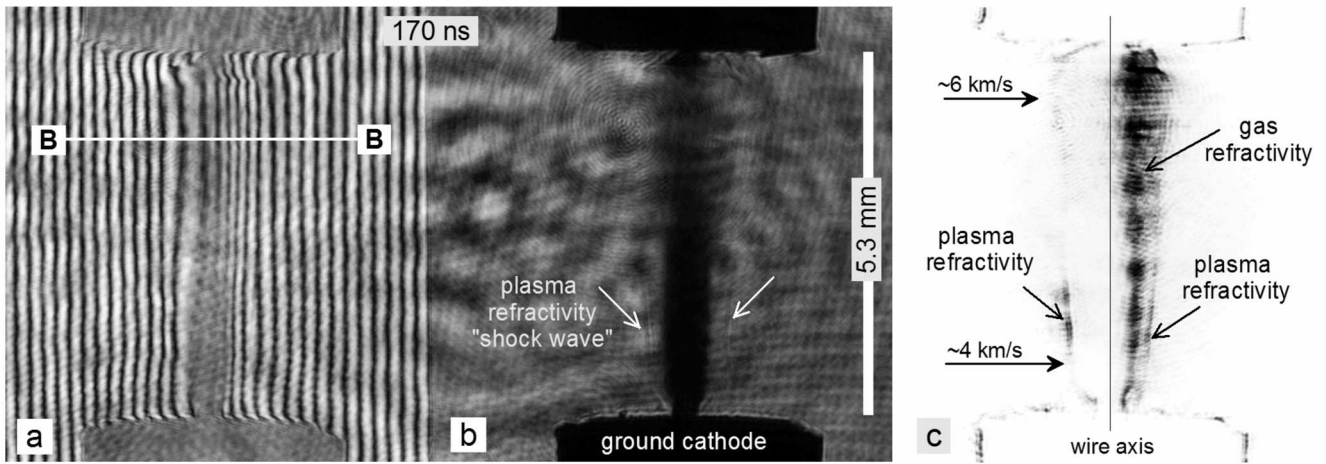


FIG. 6. Interferogram, shadowgram, and schlieren images of exploding 12 μm bare W wire.

The reconstruction of the interference phase shift (cross section B-B from Fig. 6) is presented in Fig. 7. The central part of the exploded wire with ~1.2 mm diameter exhibits a large positive phase shift $\delta_{max} \sim 1 \pm 0.1$ lines (gas-type refractivity), while the periphery produces a small negative shift with maximum value $\sim 0.14 \pm 0.1$ lines (plasma-type refractivity). Maximum expansion velocity of the detectable phase disturbance edge is ~7 km/s. Calculating the phase shift radial profile from the MHD-simulation density and ionization profiles also shows similar gas-type refractivity inside and plasma-type outside the core.

The remarkable difference in light emission wave forms for exploded coated and uncoated 12 μm W wires is presented in Fig. 8. Light from the uncoated W wire explosion starts with a narrow ~4 ns peak at the moment of voltage collapse. This is a clear signature of corona generation [4]. Coated-wire explosion shows no initial, narrow peak of light

emission, but continuously rises up to a maximum value during the first 20 ns. The amplitude of light emission from coated wire exceeds the light from uncoated wire by a factor of 11. During the first 100 ns coated wire radiates seven times more energy than uncoated.

IV. INTERFEROMETRIC DATA TREATMENT

For partially ionized plasma, the interference phase shift δ (fringes) can be written as

$$\delta(y) = \frac{1}{\lambda} \int (\mu - 1) dx = \frac{2\pi\alpha}{\lambda} \int N_a(x,y) dx - \frac{\beta}{\lambda} \int n_e(x,y) dx, \tag{1}$$

where $\beta = e^2\lambda^2 / (2\pi mc^2) = 4.49 \times 10^{-14} \lambda^2$ is the specific refractivity of free electrons, α is the dynamic atomic polariz-

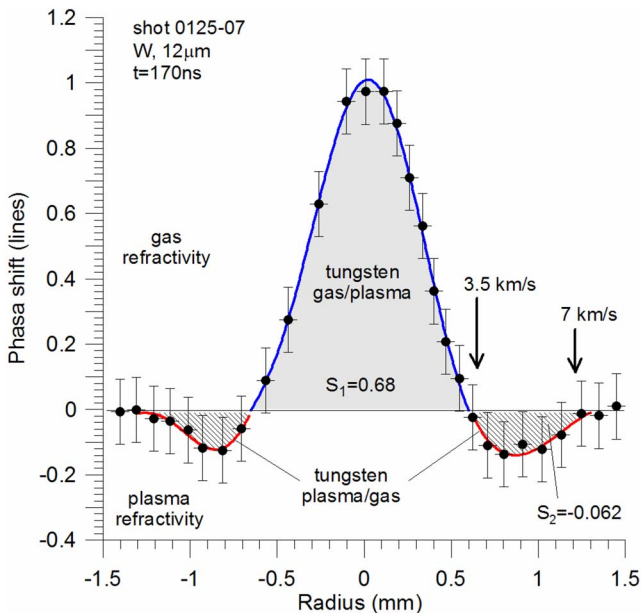


FIG. 7. (Color online) Interference phase shift in radial cross section B-B.

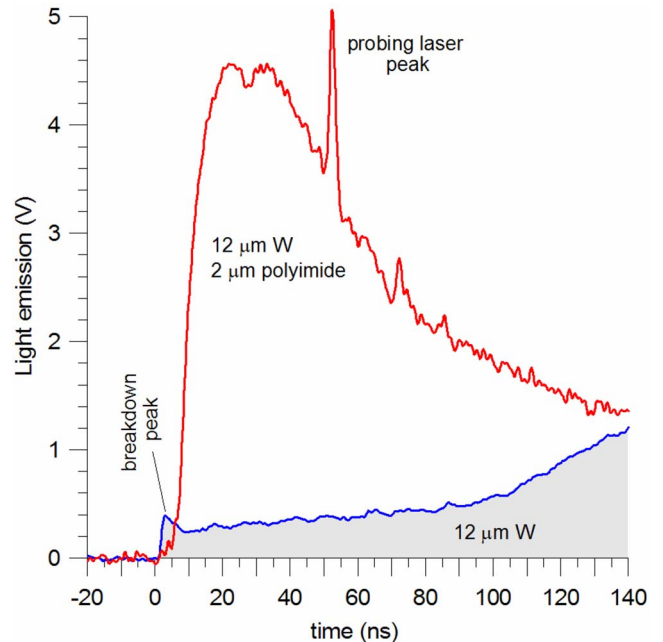


FIG. 8. (Color online) Long-time evolution of the light emission from coated and uncoated exploding W wire.

ability in cm^3 , N_a and n_e are the atomic and electron densities in cm^{-3} , X is a path length inside the plasma in cm, λ is the probing wavelength in cm, and X and Y are the directions along and perpendicular to the probing path. Ionic contribution to the phase shift is negligible.

Given the density of heavy particles (atoms and ions) $N=N_a+N_i$ and the partial ionization z , the electron and atomic densities can be written as $n_e=zN$ and $N_a=(1-z)N$. In this case the integral S of the interference phase shift along the Y direction gives

$$S = \int \delta(y)dy = \frac{1}{\lambda}[2\pi\alpha - \langle Z \rangle(2\pi\alpha + \beta)]N_{\text{lin}},$$

$$N_{\text{lin}} = \iint N dx dy, \quad (2)$$

where $\langle Z \rangle$ is the average ionization ($\langle Z \rangle \leq 1$), and N_{lin} is the lineal density of atoms and ions.

So, the average ionization of partially ionized plasma can be written as

$$\langle Z \rangle = \frac{2\pi\alpha}{2\pi\alpha + \beta} - \frac{\lambda}{2\pi\alpha + \beta} \frac{\int \delta(y)dy}{N_{\text{lin}}}$$

$$= \frac{2\pi\alpha}{2\pi\alpha + \beta} - \frac{\lambda}{2\pi\alpha + \beta} \frac{S}{N_{\text{lin}}}. \quad (3)$$

Because the exploding wire expands radially the lineal density of atoms and ions in radial cross section is invariant and equals the lineal density of atoms in the initial wire. The lineal atomic density for a $12 \mu\text{m}$ W wire is $N_{\text{lin}}=7.17 \times 10^{16} \text{ cm}^{-1}$.

To be sure that the reconstructed average ionization $\langle Z \rangle$ is accurate we did comparisons with simulation results. We used MHD profiles for $N(r)$ and $Ne(r)$ [also $Ne(r)/n$, $n=2,4,6,10$] at $t=50$ ns to calculate phase shifts and subsequently reconstruct $\langle Z \rangle$ from formula (3). Reconstructed $\langle Z \rangle$ matched the simulation average ionization to within 5%.

For totally ionized plasma ($\langle Z \rangle \geq 1$), the atomic contribution is absent, and the average plasma ionization can be calculated from formula (3) assuming formally $\alpha=0$. For a wire core in the gas state, $\langle Z \rangle=0$, and formula (3) can be used for measurements of dynamic atomic polarizability α of metal atoms similar to the *integrated-phase technique* described in Ref. [12].

The negative central area of the phase shift in Fig. 4 gives $S=-0.65$ fringes·mm. In this case, for dynamic atomic polarizability of W at wavelength 532 nm ($\alpha=15-20 \text{ \AA}^3$), the average ionization of W wire according to formula (3) is $\langle Z \rangle \sim 0.66 \pm 0.02$. The uncertainty in the atomic polarizability has little effect on the average ionization.

According to formula (3) the region with “zero refraction” ($\delta \sim 0$) for wavelength 532 nm in Fig. 3(c) has average ionization $\langle Z \rangle_{\text{zero}} \sim 0.46 \pm 0.03$. For smaller ionization ($\langle Z \rangle < \langle Z \rangle_{\text{zero}}$) the tungsten refractivity effectively turns to the gas type, for higher ionization ($\langle Z \rangle > \langle Z \rangle_{\text{zero}}$) the tungsten

refractivity turns to the plasma type. It is interesting, that in both cases we are dealing with highly ionized plasma ($\langle Z \rangle > 0.01$).

To estimate the plasma temperature we assume the condition of local thermodynamical equilibrium (LTE). At the moment of probing, the shadowgram [Fig. 3(b)] indicates that the wire diameter has increased from $12 \mu\text{m}$ to $1000 \mu\text{m}$, corresponding to a volume rise of ~ 7000 times and a drop of average atomic density from the initial $6.34 \times 10^{22} \text{ cm}^{-3}$ down to $9.1 \times 10^{18} \text{ cm}^{-3}$. For ionization $0.66 \pm 3\%$ the electron density is $6 \times 10^{18} \text{ cm}^{-3}$ and from the Saha equation the LTE temperature of tungsten plasma T is $\sim 1.2 \pm 0.1 \text{ eV}$.

Following the same procedure used for the coated wire, we estimate the average ionization of bare W wire using the interference phase shift data from Fig. 7. The total area occupied by the phase shift of Fig. 7 equals $0.68 - 2 \times 0.062 = 0.56$ fringes·mm. For dynamic atomic polarizability of W at wavelength 532 nm ($\alpha=15-20 \text{ \AA}^3$), the average ionization of W wire according to formula (3) is then $\langle Z \rangle \sim 0.28 \pm 0.04$. At the moment of probing, the phase shift profile of Fig. 7 indicates that the wire diameter has increased from $12 \mu\text{m}$ to $\sim 2400 \mu\text{m}$, corresponding to a volume rise of ~ 40000 times and a drop of average atomic density from the initial $6.34 \times 10^{22} \text{ cm}^{-3}$ down to $1.6 \times 10^{18} \text{ cm}^{-3}$. In this case the average electron density becomes $\langle n_e \rangle \sim 0.45 \times 10^{18} \text{ cm}^{-3}$. For ionization 0.28 and electron density $4.5 \times 10^{17} \text{ cm}^{-3}$ the estimated LTE temperature of tungsten plasma T is $\sim 0.63 \pm 0.1 \text{ eV}$.

V. MHD SIMULATION OF WIRE EXPLOSION

Figure 9 demonstrates the results of an MHD simulation of the coated $12 \mu\text{m}$ W wire (using the current wave form from shot 0222-02). The MHD simulations employed the MACH2 code [13] with Lee-More-Desjarlais electron transport [14] and SESAME equation of state tables [15]. Figure 9(a) shows the radial profile of atomic and ionic density, temperature, and ionization at 9 ns and 50 ns after the current start. We observe a narrow 30% rise of the edge temperature at 9 ns (5.8–7.6 eV) and a wider more than 100% rise at 50 ns (1–2.1 eV). The temperature profiles also clearly indicate the absence of corona. The mean temperature is consistent with the LTE temperature deduced from the interferometry (1.2 eV) for the coated wire. The density profiles show a bump on the periphery corresponding to the low-temperature polyamide coating. At both times the coating has significantly lower temperature than the metal core. Figure 9(b) shows the evolution of the wire diameter between two points: where the atomic and ionic density is 1/10 of maximum, and at the edge of the dielectric coating. The temporal variation of the temperature at the center of the wire and at the periphery is also presented. At any time the maximum temperature occurs at the periphery and the minimum on the axis. Hence, these two histories show the temperature variation across the wire at any time. According to the MHD simulation, the wire core temperature reaches a maximum value of 5.8–7.6 eV at 9 ns after the current start. Subsequently, the wire expands and cools down to 1–2.1 eV at 50 ns. The wire expands with velocity from 12 km/s (1/10 of

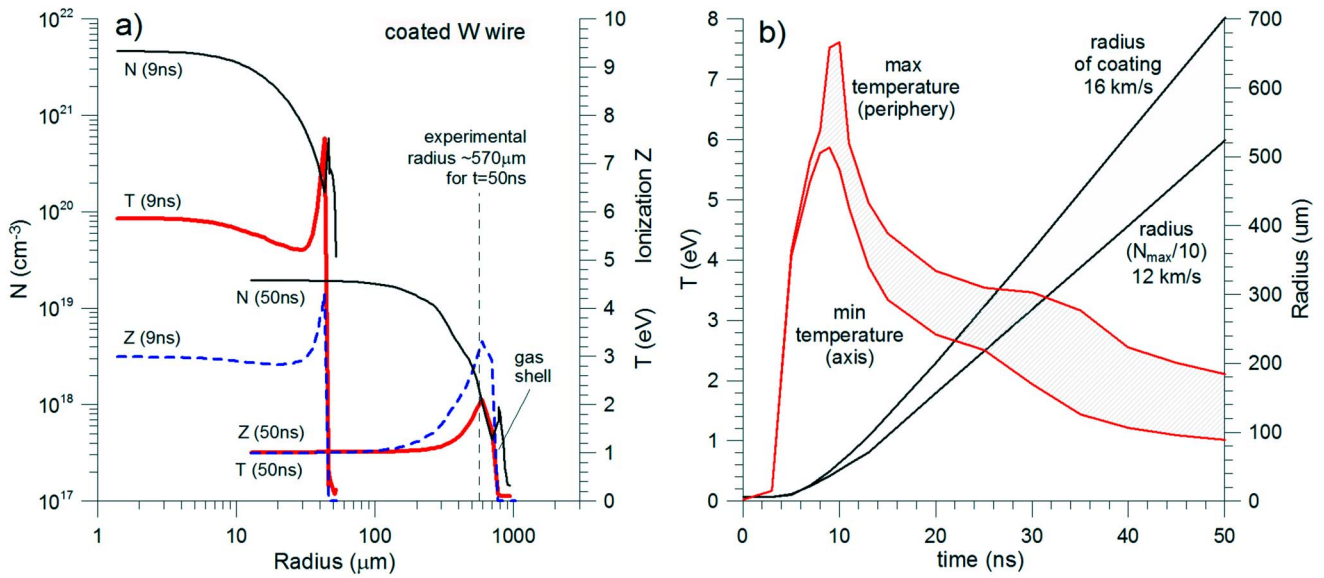


FIG. 9. (Color online) MHD-simulation results for explosion of 12 μm W wire with 2 μm polyimide coating: (a) Radial distribution of the density, temperature, and ionization for 9 ns and 50 ns. (b) Evolution of wire radius and temperature.

maximum density) up to 16 km/s (boundary of coating). This matches the expansion velocity determined from the optical data of Fig. 3.

An MHD simulation of the bare 12 μm W wire (using the current wave form from shot 0125-07) is presented in Fig. 10. Figure 10(a) shows the radial profile of atomic and ionic density, temperature, and ionization at 5 ns and 50 ns after the current start. We observe a two-phase behavior of the exploding wire: high-density and low-temperature core (3.5 eV at $t=5$ ns) accompanied by a low-density and high-temperature corona (~ 50 eV at $t=5$ ns). After the corona forms and rapidly expands, the current flows mostly through the less resistive corona and can no longer heat the wire core. Figure 10(b) shows the evolution of the wire diameter between two points: where the atomic and ionic density is 1/10

of maximum, and at the edge of the corona. Figure 10(b) also shows the evolution of the maximum wire-core and corona temperatures. According to MHD simulation, the wire-core temperature reaches its maximum value of 3.5 eV at 5 ns after the current start. The corona temperature reaches its maximum of ~ 50 eV also at 5 ns, the time of initial corona generation. Much later, corresponding to the experimental probing time, the core temperature is ~ 0.5 eV, consistent with the experimentally estimated temperature (0.6 eV). The wire core expands with velocity ~ 6.5 km/s (where $N_{\text{max}}/10$), while the corona expands with initial high velocity ~ 40 km/s. The simulation core expansion velocity is in good agreement with the core expansion velocity (4–6 km/s) and the detectable phase disturbance (~ 7 km/s) observed in the optical data of Fig. 6.

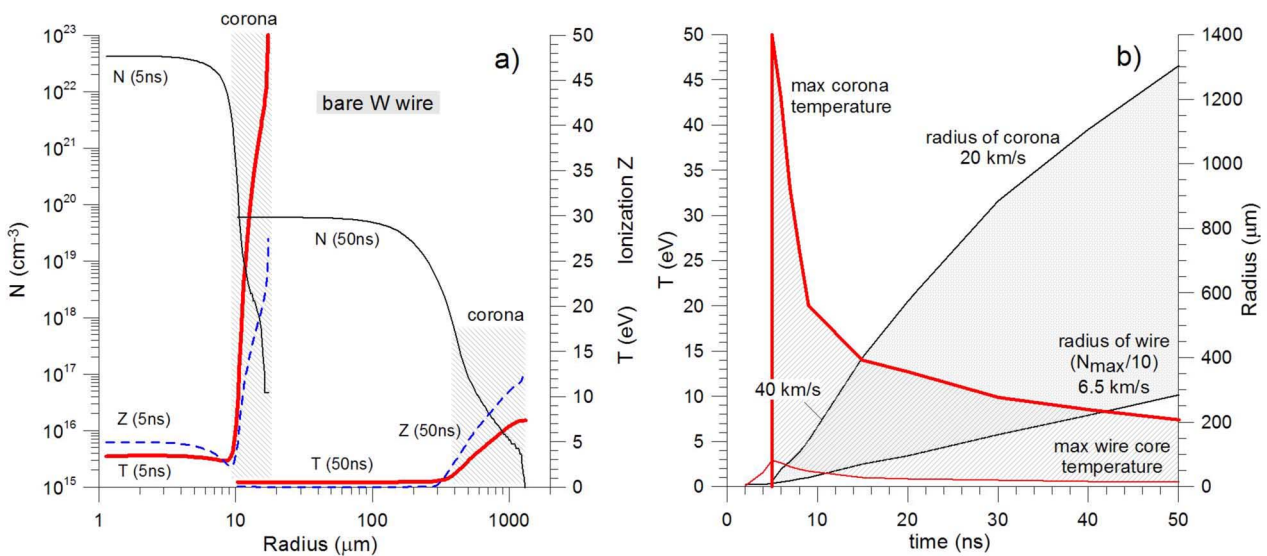


FIG. 10. (Color online) MHD-simulation results for explosion of bare 12 μm W wire: (a) Radial distribution of the density, temperature, and ionization for 5 ns and 50 ns. (b) Evolution of wire radius and temperature.

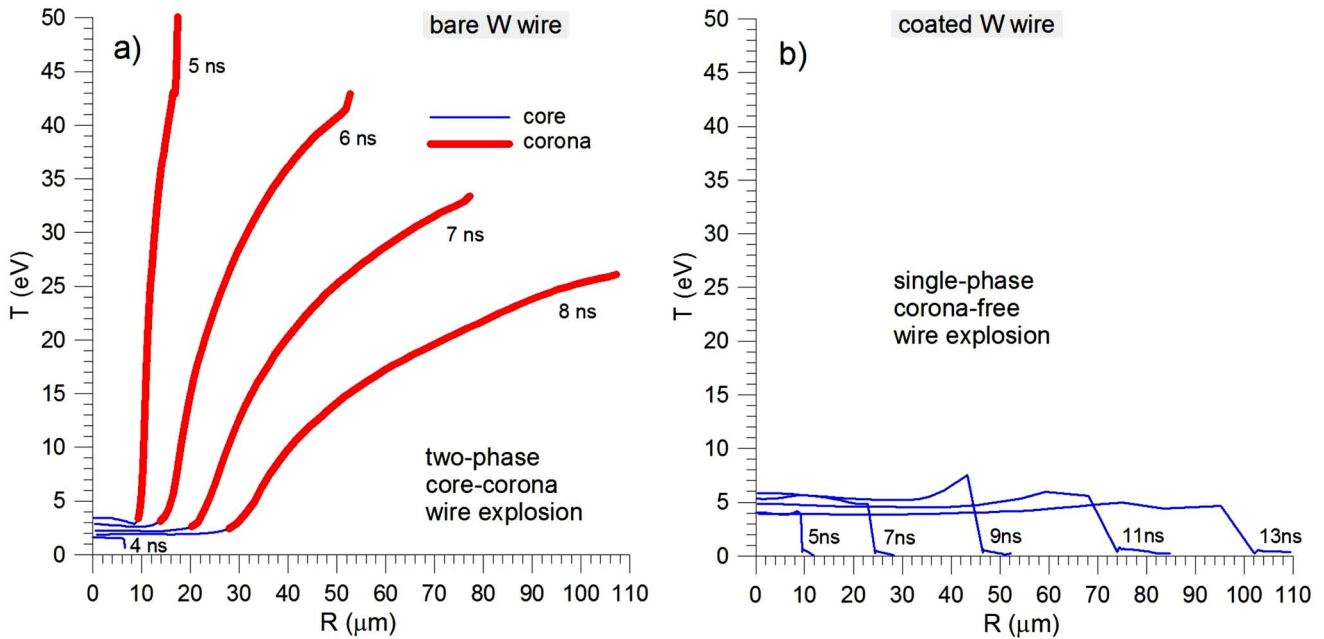


FIG. 11. (Color online) MHD-simulation results: Radial distribution of temperature for bare (a) and coated (b) 12 μm W wire at five different times.

Radial distributions of the temperature at five moments of time for bare and coated wires are presented in Fig. 11. This (a)-(b) comparison throws the difference between bare and coated-wire explosions into sharp relief: bare wire explodes in Fig. 11(a) with the generation of low-density corona (two-phase explosion); coated wire explodes in Fig. 11(b) without corona (single-phase explosion).

Figure 12 demonstrates radial distributions of density (ions and atoms), temperature, and linear density of thermal energy at $t=9$ ns for exploding bare and coated W wires. At the same moment of time coated wire contains almost five times more thermal energy than bare. The thermal energy is

distributed between core and corona in a bare-wire explosion. At $t=9$ ns the corona contains $\sim 15\%$ of the total energy. At the moment of corona generation ($t=5$ ns) the corona contains only $\sim 2\%$ of the total thermal energy, even though the coronal temperature is high, ~ 50 eV. In a coated-wire explosion the core contains all the thermal energy.

The radial distribution of the current and relative wire mass at 20 ns for bare (a) and coated (b) exploding 12 μm W wires are presented in Fig. 13. For the exploding bare wire in Fig. 13(a) 95% of the wire mass contains only $\sim 0.7\%$ of the total current. The main current $\sim 99\%$ flows through the

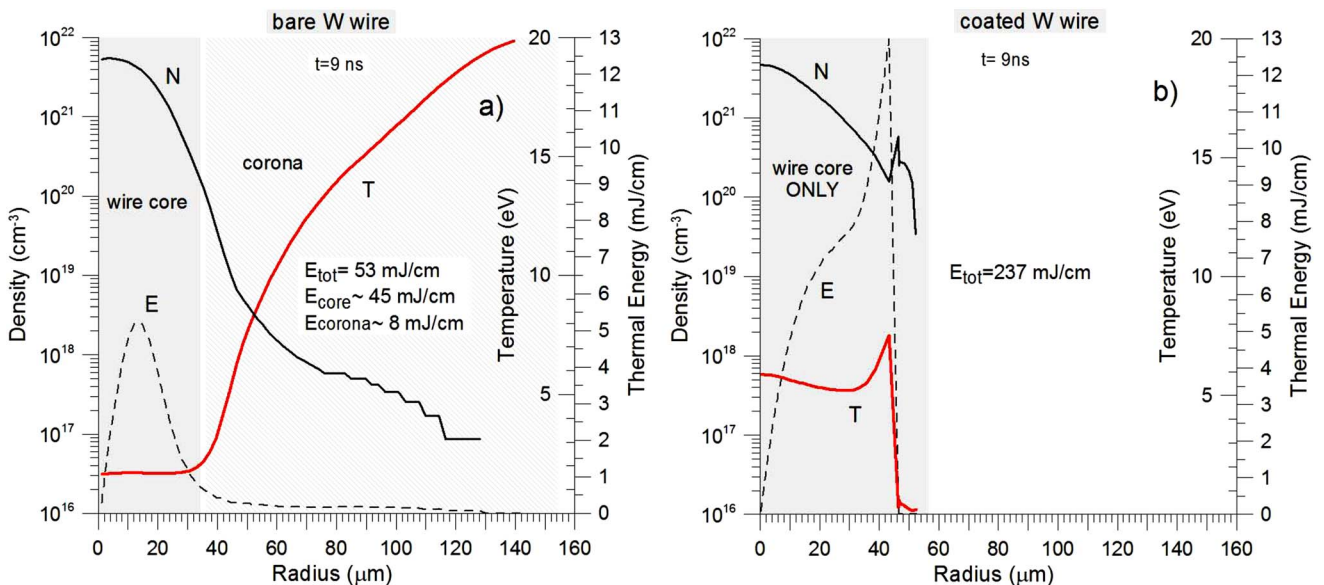


FIG. 12. (Color online) MHD-simulation results: Radial distribution of density, temperature, and linear density of thermal energy for bare (a) and coated (b) 12 μm W wire at $t=9$ ns.

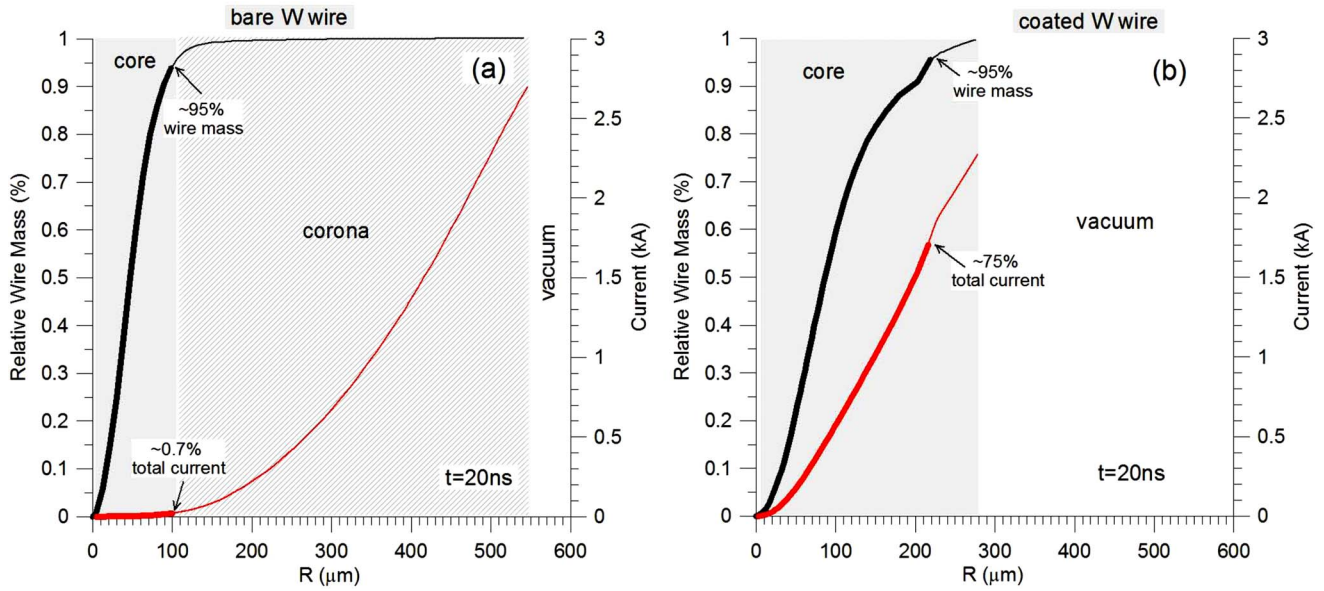


FIG. 13. (Color online) MHD-simulation results: Radial distribution of wire mass and current for coated (a) and uncoated (b) $12 \mu\text{m}$ W wires at $t=20 \text{ ns}$.

external low-density corona. This provides a clear indication that once the corona forms, Joule heating of the predominant mass (wire core) essentially stops. Breakdown and corona generation of uncoated metal wire acts like a fast radial switch, which stops current flow through the wire core. Later, wire-core vaporization occurs due to heat transport and radiation from the hot surrounding corona. For the exploding coated wire in Fig. 13(b) the total current flows through the wire core, Joule heating the predominant mass. Figure 13(b) shows that 95% of the wire mass contains 75% of the total current. An appropriately coated W wire explodes as a single-phase object (no corona), so all current flows through the wire core, heating it without interruption.

VI. DISCUSSION

Experimental and computational investigation shows the remarkable difference between explosion of coated and uncoated tungsten wires in vacuum. Unlike the breakdown-related phenomena always observed in bare-wire explosions [8], our coated-wire experiments show: (1) very large light emission without early peak, (2) cylindrical shape of expansion (conical shape is typical for positive-polarity bare-wire explosion), (3) abnormally long resistive time, and (4) extraordinarily high core expansion velocity ($\sim 18 \text{ km/s}$) due to large energy deposition ($\sim 130 \text{ eV/atom}$). Our earlier report of coated-W wire explosion [6] relied on the voltage and current wave forms, laser shadowgraphy, and on differences in the light emission wave forms in conjunction with the MHD simulations to infer the corona-free explosion of coated wire. The MHD predictions in Ref. [6] (two-phase explosion of bare W wire, and single-phase explosion of coated-W wire) have now been firmly established experimentally by the addition of interferometry and schlieren imaging. For fast energy deposition, the coating dynamically tamps the metal that would normally vaporize and ionize; the coat-

ing thereby prevents corona formation. In the absence of a core-corona structure the exploding coated wire evolves as a single-phase object, Joule heating to a plasma state. This qualitatively differs from bare-wire explosions in which a corona takes all the current from the wire core and the bare-wire core then stops Joule heating (kind of a radial switch). For smaller current rate ($dI/dt < 100 \text{ A/ns}$) the bare W wire core can stay in liquid or even solid state due to earlier termination of Joule heating by the corona [8]. Slow-exploding coated-W wire demonstrates corona generation [6]. The polarity effect is absent for fast exploding coated-W wire, similar to explosion in the air [6].

Corona-free explosion of a single wire could be an alternative for x-ray radiating wire-array z pinches [16]. The main goal of the wire-array z pinch is to generate an axial hot, dense plasma column. In this paper we have demonstrated how a single exploding coated wire can produce the restricted cylindrical plasma column without surrounding low-density plasma. A two-stage current would entail first a very fast prepulse current (1 kA/ns) to explode the single coated wire followed by a large main current for magnetic compression, heating, and conversion to x-ray energy. With this approach one essentially replaces the ablation phase of many ~ 300 thin wires by an extended resistive phase of a single thick wire with dielectric coating. For example, to keep the same mass, 300 wires of $5 \mu\text{m}$ diameter can be replaced by a single wire of $\sim 87 \mu\text{m}$ diameter. Additional benefit could be derived from doping the dielectric coating with deuterium. This convenient placement would exploit the heating peak on the periphery of the plasma column (Fig. 9). Detailed discussion of these possibilities is outside the scope of the present paper, and will be the topic for a future publication.

VII. CONCLUSION

The $2 \mu\text{m}$ polyimide coating of thin W wire dramatically changes the explosion process. The coating effectively tamps

the wire during the nanosecond time scale. During the explosion the temperature of the polyimide coating remains significantly less than the temperature of the metal core, totally suppressing the current-shunting corona. This regime of explosion allows the creation of a perfectly cylindrical plasma column, without surrounding low-density plasma.

The extremely high current rate we used ($dI/dt \sim 1000$ A/ns) allowed the transformation of the tungsten core to the plasma state even for uncoated wire. The fundamental difference between coated and uncoated W explosions with this high current rate was the absence of corona for coated wire. Without an expanding corona to take

the current away from the core, the core in a coated W wire explosion can attain greater energy through prolonged Joule heating leading to a perfectly cylindrical hot, dense plasma column. Moreover, an intrinsically three-dimensional (3D) problem becomes two dimensional (2D).

ACKNOWLEDGMENTS

Sandia is a multiprogram laboratory operated by the Sandia Corporation, a Lockheed Martin Co., for the U.S. DOE under Contract No. DE-AC04-94AL85000.

-
- [1] F. D. Bennett, in *Progress in High Temperature Physics and Chemistry*, edited by C. A. Rouse (Pergamon Press, New York, 1968), Vol. 2, p. 3.
- [2] S. V. Lebedev and A. I. Savvatimskii, *Sov. Phys. Usp.* **27**, 749 (1984).
- [3] V. A. Burtsev, N. V. Kalinin, and A. V. Luchinski, *Electrical Explosion of Conductors and Its Application in Electro-Physical Installations* (Energoatomizdat, Moscow, 1990) (in Russian).
- [4] G. S. Sarkisov, S. E. Rosenthal, K. R. Cochrane, K. W. Struve, C. Deeney, and D. H. McDaniel, *Phys. Rev. E* **71**, 046404 (2005).
- [5] N. N. Sobolev, *Zh. Eksp. Teor. Fiz.* **17**, 986 (1947) (in Russian).
- [6] G. S. Sarkisov, S. E. Rosenthal, K. W. Struve, and D. H. McDaniel, *Phys. Rev. Lett.* **94**, 035004 (2005).
- [7] D. B. Sinars, T. A. Shelkovenko, S. A. Pikuz *et al.*, *Phys. Plasmas* **7**, 429 (2000).
- [8] G. S. Sarkisov, K. W. Struve, and D. H. McDaniel, *Phys. Plasmas* **12**, 052702 (2005).
- [9] L. A. Vasil'ev, *Schlieren Methods* (Israel Program for Scientific Translation Ltd. and KETER Inc., New York, 1971), p. 25.
- [10] G. S. Sarkisov, *Instrum. Exp. Tech.* **39**, 727 (1996).
- [11] G. S. Sarkisov, P. V. Sasorov, K. W. Struve, D. H. McDaniel, A. N. Gribov, and G. M. Oleinik, *Phys. Rev. E* **66**, 046413 (2002).
- [12] G. S. Sarkisov, I. L. Beigman, V. P. Shevelko, and K. W. Struve, *Phys. Rev. A* **73**, 042501 (2006).
- [13] M. H. Frese, *MACH2: A Two-Dimensional Magnetohydrodynamic Simulation Code for Complex Experimental Configurations* (NumerEx, Albuquerque, 1990).
- [14] M. P. Desjarlais, *Contrib. Plasma Phys.* **41**, 267 (2001).
- [15] K. S. Holian, LANL Report No. LA-10160-MS (1984).
- [16] M. K. Matzen, *Phys. Plasmas* **4**, 1519 (1997).